Software-defined radio prototype for fast-convolution-based filtered OFDM in 5G NR

Software-Defined Radio Prototype for Fast-Convolution-Based Filtered OFDM in 5G NR

Selahattin Gökceli*, Toni Levanen*, Juha Yli-Kaakinen*, Matias Turunen*, Markus Allen*,
Taneli Riihonen*, Arto Palin†, Markku Renfors*, and Mikko Valkama*
*Tampere University, Department of Electrical Engineering, Tampere, Finland
†Nokia Mobile Networks, Tampere, Finland

***Abstract*—In this work, we provide first-in-class measurement results for fast-convolution-based filtered orthogonal frequency-division multiplexing (FC-F-OFDM) processing implemented on a universal software radio peripheral (USRP) software-defined radio (SDR). The fast-convolution-based processing offers a highly efficient and flexible filtered OFDM scheme allowing to achieve high spectral utilization in different channel bandwidths. Through the SDR implementation and transmitter spectrum emission measurements, we show that FC-F-OFDM allows to increase spectrum utilization compared to the fifth generation new radio (5G NR) Release-15 requirements. Furthermore, considering the out-of-band emission masks and adjacent-channel-leakage-ratio requirements, FC-F-OFDM provides a larger interference margin than well-known windowed overlap-and-add OFDM processing.**

***Keywords*—5G New Radio (NR), Fast Convolution, Filtered OFDM, Physical Layer, Prototype, SDR.**

I. Introduction

The fifth generation new radio (5G NR) mobile communication systems are expected to increase data rates significantly by supporting wider channel bandwidths and new carrier frequencies [1]–[3]. The latency of the physical layer is reduced by the support of multiple subcarrier spacings (SCSs) in different frequency ranges and operating bands as well as by mini-slot-based transmission. The 5G NR supports two frequency ranges (FRs), where FR1 is for operation from 450 MHz to 6 GHz and FR2 is for operation from 24.25 GHz to 52.6 GHz carrier frequencies [4]. One of the main design targets for 5G NR has been to improve spectral utilization when compared to the 90 % utilization typically achieved in long-term evolution (LTE) systems. Depending on the used SCS and channel bandwidth, a 5G NR system may actually result in lower spectral utilization, e.g., the spectral utilization of a 5 MHz channel bandwidth operating with 30 kHz SCS with a maximum of 11 active physical resource blocks (PRBs) is only 79.2 %, which is computed based on the transmission bandwidth configuration parameters defined in [4]. Increasing spectrum utilization will improve the maximum throughput per channel bandwidth while imposing more stringent requirements for the channel filtering or time-domain windowing used to constrain spectral emissions.

The physical layer (PHY) radio access of 5G NR in downlink (DL) and uplink (UL) is based on cyclic-prefix (CP) orthogonal frequency-division multiplexing (OFDM) due to its various benefits. For example, CP-OFDM provides straightforward multiple-input multiple-output (MIMO) support and superior flexibility in the frequency-domain allocation granularity, especially in the case of discontinuous UL allocations, which are basically not supported by LTE. Due to the high diversity of 5G NR applications, the flexibility and performance of the waveform processing solution selected to improve the spectral containment of the underlying waveform is crucial. In this study, CP-OFDM-based UL transmission is targeted as it is more relevant for high-throughput use cases. On the other hand, DFT-spread precoding is not considered, as it is intended only for coverage-limited user equipments (UEs).

Different CP-OFDM waveforms based on filtering and time-domain windowing have been studied extensively over the recent years [5]–[10]. Among the CP-OFDM waveform variants, subband filtering-based waveforms have received significant attention due to their flexibility and spectral containment advantages. The time-domain implementations of flexible filtering solutions are quite complex and optimization for multiple different subbands, bandwidth parts, or channel bandwidths is not trivial. For this reason, the fast-convolution-based filtered-OFDM (FC-F-OFDM) waveform was proposed in [7], [11]. It enables an efficient subband processing mechanism by combining filtering that is based on fast convolution (FC) with a CP-OFDM waveform. This allows simple and flexible spectral shaping for a wide range of different passband widths and provides very good spectral containment and transmitter (Tx) error vector magnitude (EVM) performance. Furthermore, applying FC-F-OFDM in the Tx (receiver (Rx)) is completely transparent processing such that it does not necessitate any special Rx (Tx) processing and is thus compatible with conventional CP-OFDM Rx (Tx) [12].

In this study, the first measurement results for a universal software radio peripheral (USRP)-based software-defined radio (SDR) prototype implementation of the FC-F-OFDM are presented, including out-of-band (OOB) emission and adjacent-channel-leakage-ratio (ACLR) measurements following the latest 5G NR UE requirements for FR1 [4]. The FC-F-OFDM performance is compared with weighted overlap-and-add (WOLA)-based OFDM (WOLA-OFDM) [8], [9] operating in the same SDR platform. Due to its simplicity, WOLA-OFDM is commonly assumed for UE Tx and Rx processing and is therefore considered as the main reference in performance comparisons. In addition, reference numerical evaluation results are shown with a good alignment to the real-time measurements. To highlight the benefits of FC-F-OFDM, we also push the transmission bandwidth configuration sizes beyond the 5G NR Release-15 requirements, and show that both candidate waveforms allow to achieve larger spectral utilization, whereas FC-F-OFDM results in smaller spectral leakage and, therefore, increased interference margin with respect to the OOB emission masks.

The paper is organized as follows. In Section II, the USRP-based SDR prototype testbed and the evaluated 5G NR transmitter emission requirements are explained. Next, in Section III, the considered waveform processing techniques applied on top of the CP-OFDM waveform are described in

detail. Then, in Section IV, the real-time USRP-based SDR prototype measurement results are analyzed and discussed together with supporting numerical evaluations. Finally, the conclusions are drawn in Section V.

II. USRP-Based SDR Prototype Description and 5G NR Emission Requirements

A. SDR Prototype Measurement Setup Description

A high-level description of the Tx implementation and the USRP-based SDR prototype measurement setup is illustrated in Fig. 1. The main focus of this paper is in UL scenarios, modeling UE devices' transmission and evaluating the corresponding 5G NR output RF spectrum emission requirements. Assuming a power class 3 device, the maximum UE output power is 23 dBm [4]. Noting the 3 dB maximum power reduction allowed for a QPSK-modulated full-band CP-OFDM signal, we concentrate in this paper to achieve 20 dBm radiated power. In addition, we assume that there is 4 dB of additional loss between the power amplifier (PA) and the antenna port, leading to PA output power requirement of 24 dBm. In UL, it is of great importance to maximize the Tx power to improve UE's power efficiency and also the system throughput. Operating with lower PA output power levels leads to more linear behavior by the PA, thus providing performance similar to the provided numerical results further emphasizing the improved spectral containment achieved with FC-F-OFDM.

Accordingly, the baseband waveform processing is realized on the host processor and generated data is transferred to the USRP device via PCIe connection. The RF modulation and the pre-amplification are implemented by using a NI USRP-2954R RIO device [13], which supports instantaneous bandwidth of 120 MHz and the considered carrier frequency of 3.5 GHz. The USRP hardware is assumed to provide similar impairments as a medium-priced UE and therefore it is selected to model a realistic UE transmitter chain. Then by using a RF cable, the output signal from the USRP RIO device is inserted to a 3 dB power splitter which divides the signal between a Rohde & Schwarz NRP-Z11 power meter and an external PA. The used power meter supports an input power up to 23 dBm and frequency range of 10 MHz to 8 GHz [14]. The USRP device has a varying transmission power level per signal realization and in order to accurately configure the PA input power level, the power meter was included in the measurement setup to ensure that the average input power to the external PA is not fluctuating more than 0.2 dB during the real-time measurements. In this scenario, the internal PA of the USRP RIO device acts as a pre-amplifier to drive the external PA.

Because the used USRP RIO device is not able to provide the required output power, it is connected to an external ZHL-4240+ PA, which is a wideband PA providing 42 dB gain with a high third-order output intercept point (OIP3) of 38 dBm in the operating carrier frequency of 3.5 GHz and supports operation in frequencies from 0.7 GHz to 4.2 GHz [15]. After the external PA, an additional 34 dB attenuator was applied to protect a vector signal transceiver (VST) module, acting as the measurement Rx, and to include the 4 dB additional loss typically assumed for UEs between the PA and the antenna port. As we are targeting to evaluate the 5G NR OOB emissions and NR ACLR, a high quality Rx with a large instantaneous bandwidth support is required. Therefore, we have used NI PXIe-5840 VST as the measurement Rx, which can provide

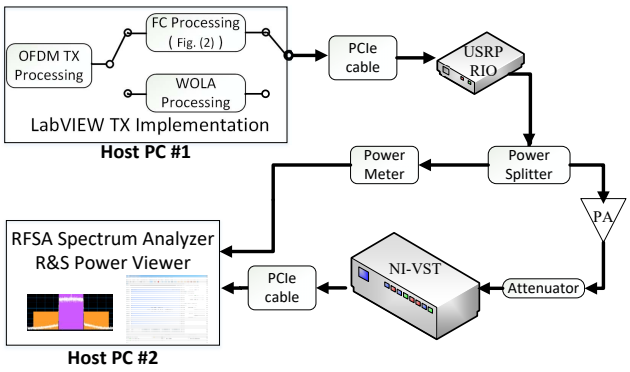

Fig. 1: Block diagram of the considered USRP-based SDR prototype measurement setup.

instantaneous bandwidth up to 1 GHz [16]. While evaluating the Tx output RF emissions, the devices are connected with a coaxial cable. Received data is then transferred to the host computer via 1 GB PCIe connection for spectrum analysis. As the software tool, LabVIEW is used by utilizing corresponding hardware and communications libraries.

B. 5G NR Transmitter RF Emission Requirements

The NR ACLR is defined as the ratio of the filtered mean power of the operating NR channel to the filtered mean power of an adjacent NR channel [4]. The channel powers are measured by assuming a rectangular filter with measurement bandwidths corresponding to 4.515 MHz, 19.095 MHz, and 98.310 MHz in channel bandwidths 5 MHz, 20 MHz, and 100 MHz, respectively [4]. These values basically correspond to the maximum transmission configuration size defined for each bandwidth plus one SCS based on the smallest SCS supported in that channel bandwidth. The reason for the additional SCS is due to the configurable half of a SC shift in 5G NR UL. To follow similar logic in evaluating the ACLR in the extreme spectrum utilization examples, in accordance with definitions given in [4], we have used measurement bandwidths 4.875 MHz, 19.635 MHz, and 99.390 MHz with channel bandwidths 5 MHz, 20 MHz, and 100 MHz, respectively.

The 5G NR OOB spectrum emission mask for UEs operating in FR1 is defined in [4]. Basically, the spectrum emission mask contains two different regions. Within distance of 1 MHz from the channel edge, the bandwidth of the measurement filter corresponds to 1 % of the channel bandwidth and the spectrum emission limit is −13 dBm for channel bandwidths from 5 MHz to 40 MHz, and for larger channel bandwidths the measurement filter bandwidth is 30 kHz and the emission limit is −24 dBm. For distances larger than 1 MHz from the channel edge, the used measurement bandwidth is 1 MHz and the attenuation target depends on the distance to the channel edge and the channel bandwidth as defined in [4, Table 6.5.2.2-1].

III. Evaluated Waveform Processing Techniques

A. FC-F-OFDM Processing

The efficient implementation of a high-order filter through frequency-domain processing is the core component of the multirate processing used to implement FC-F-OFDM [7]. At the transmitter side, in general case, M subband signals $\mathbf{x}_m$

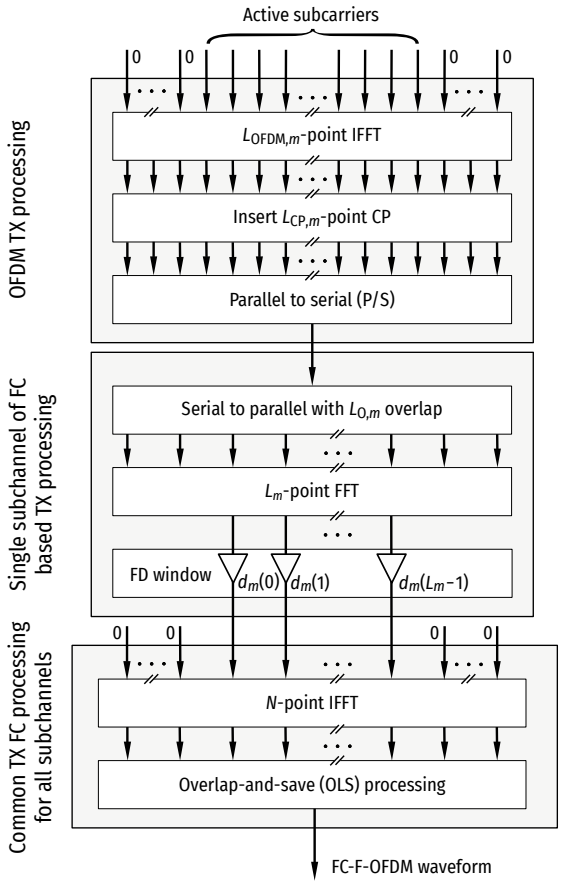

Fig. 2: Block diagram for the FC-F-OFDM transmitter processing of the mth subband.

with subband index $m = 0, 1, \ldots, M-1$, are generated and filtered by the FC processing. Figure 2 illustrates the Tx-side processing for mth subband. The time-domain OFDM signal $\mathbf{X}_{\mathrm{OFDM},m}$ is obtained from frequency-domain symbols $\mathbf{X}_m$ with $L_{\mathrm{ACT},m}$ active subcarriers by taking the $L_{\mathrm{OFDM},m}$-point IFFT. Then, a CP of length $L_{\mathrm{CP},m}$ is inserted and the resulting CP-OFDM signal $\mathbf{X}_{\mathrm{CP\text{-}OFDM},m}$ is converted from parallel to serial for FC processing. Let $\mathbf{x}_m = \mathrm{vec}(\mathbf{X}_{\mathrm{CP\text{-}OFDM},m})$ denote the column vector formed by vertically stacking the columns of $\mathbf{X}_{\mathrm{CP\text{-}OFDM},m}$.

In the FC processing part, each of the M signals to be transmitted is first segmented into overlapping processing blocks of length L_m with overlap of $L_{\mathrm{O},m}$ samples. Let us denote the non-overlapping part by $L_{\mathrm{S},m} = L_m - L_{\mathrm{O},m}$ and the overlap factor by $\lambda = 1 - L_{\mathrm{S},m}/L_m$. Then, each input block is transformed to frequency domain using L_m-point FFT. The frequency-domain bin values of each converted subband signal are multiplied by the frequency-domain window $\mathbf{d}_m$ corresponding to the FFT of the finite-length linear filter impulse response. Finally, the weighted signals are combined and converted back to time domain using N-point IFFT and the resulting time-domain output blocks are concatenated using the overlap-and-save principle such that the output blocks are truncated to $N_{\mathrm{S}} = (1-\lambda N)$ samples.

In the structure of Fig. 2, the OFDM Tx processing module generates samples for the overall symbol duration of $L_{\mathrm{OFDM},m} + L_{\mathrm{CP},m}$. The FC-filtering process increases the sampling rate by the factor of $I_m = N/L_m = N_{\mathrm{S}}/L_{\mathrm{S},m}$. By adjusting the forward and inverse transform lengths, the sampling rate conversion factor can be flexibly configured. However, in this study, we concentrate on the channel filtering use case, where the sampling rates in the input and output of the FC processing are the same, essentially meaning that the inverse and forward transform lengths are the same.

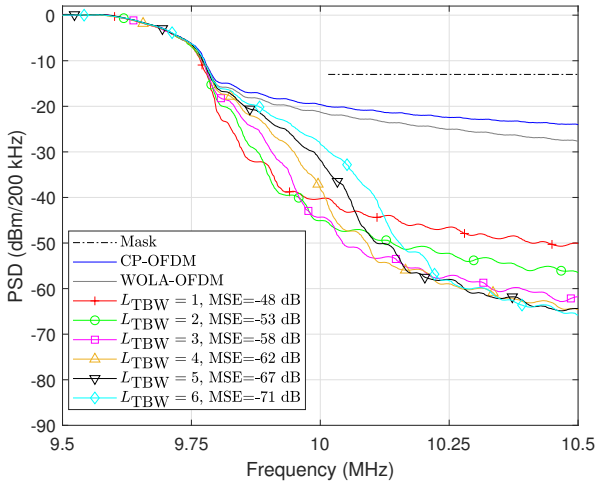

Fig. 3: Example power spectral densities (PSD) close to channel edge for FC-F-OFDM waveforms with different number of transition-band bins for 20 MHz channel with 60 kHz SCS and 27 PRB allocation. Responses for plain CP-OFDM waveform and WOLA-OFDM waveform are shown as a reference.

In the Tx processing, i.e., FC synthesis filter bank case, the block processing of the mth CP-OFDM subband signal $\mathbf{x}_m$ for the generation of a high-rate subband waveform $\mathbf{w}_m$ can be represented as $\mathbf{w}_m = \mathbf{F}_m\mathbf{x}_m$, where $\mathbf{F}_m$ is the block transform matrix with R_m blocks, defined as $\mathbf{F}_m = \mathrm{diag}\left(\mathbf{F}_{m,0}, \mathbf{F}_{m,1}, \ldots, \mathbf{F}_{m,R_m-1}\right)$. The $N_s \times L_m$ submatrices $\mathbf{F}_{m,r}$ can be decomposed as

$$\mathbf{F}_{m,r} = \mathbf{S}_N\mathbf{W}_N^{-1}\mathbf{M}_{m,r}\mathbf{D}_m\mathbf{P}_{L_M}^{(L_m/2)}\mathbf{W}_{L_m}, \tag{1}$$

where $\mathbf{W}_{L_m}$ and $\mathbf{W}_N^{-1}$ represent the $L_m \times L_m$ DFT matrix and $N \times N$ inverse DFT matrix, respectively. Moreover, $\mathbf{P}_{L_M}^{(L_m/2)}$ represents the DFT-shift matrix obtained by cyclically left shifting the $L_m \times L_m$ identity matrix by $L_m/2$ positions and $\mathbf{D}_m$ denotes the $L_m \times L_m$ diagonal matrix that contains the frequency-domain window weights of the mth subband on the diagonal. Matrix $\mathbf{M}_{m,r}$ of size $N \times L_m$ maps input's L_m frequency-domain bins to output signal's frequency-domain bins $(c_m - \lceil L_m/2 \rceil + l)_N$ for $l = 0, 1, \ldots, L_m - 1$. Here, c_m and $()_N$ represent the center of the mth subband and modulo-N operation, respectively. Furthermore, to provide phase continuation between consecutive processing blocks, the matrix $\mathbf{M}_{m,r}$ rotates the phases of the blocks by $\theta_m(r) = \exp(j2\pi r\theta_m)$, where $\theta_m = c_m L_{s,m}/L_m$. As the last operation of the FC-processing, the $N_s \times N$ selection matrix $\mathbf{S}_N$ selects the required N_s samples corresponding to overlap-and-save processing.

Fig. 3 shows a concrete example of the FC-F-OFDM spectral containment performance with different transition bandwidths, defined through the number of non-trivial transition band weights ($L_{\mathrm{TBW},m}$). In this example, 200 kHz measurement bandwidth is used to evaluate the power spectral densities (PSDs). The transition-band weights are obtained from the

TABLE I: The main physical layer parameters

Parameter	Value
Carrier frequency [GHz]	3.5
Transmit power [dBm]	24
Channel bandwidth [MHz]	5 / 20 / 100
Subcarrier spacing (SCS) [kHz]	15 / 30 / 60
Physical resource block (PRB) size in subcarriers	12
CP-OFDM symbols per slot	14
Number of slots averaged in the measurements	1000
FC-F-OFDM: overlap factor	1/2
FC-F-OFDM: Number of transition band weights ($L_{\mathrm{TBW},m}$)	4
FC-F-OFDM: Transition band response	raised cosine
WOLA-OFDM: Window roll-off	0.02
WOLA-OFDM: Window slope response	raised cosine

sampled raised-cosine response defined below in (2). The passband weights and stopband weights are set to one and zero, respectively. A higher value of $L_{\mathrm{TBW},m}$ reduces the in-band distortion experienced by the edge subcarriers and increases the minimum stopband attenuation. The average mean-squared-error (MSE) measured following the 5G NR requirements [4] is also provided in the line specific labels highlighting the very low distortion induced by FC filtering on the transmitted signal. As $L_{\mathrm{TBW},m}$ increases, the minimum interference margin between the OOB emission mask and the filtered waveform is reduced, as exemplified in Fig. 3. As it can be seen, $L_{\mathrm{TBW},m} = 4$ provides a good compromise between these two factors and therefore this value was selected for this study. Dedicated optimization routines to improve the performance beyond raised-cosine designs are presented in [7], but the numerology-specific optimization and performance analysis are beyond the scope of this paper. Additional information on the effect of the FC overlap factor and different transform sizes, and a complexity analysis of FC-F-OFDM can be found in [7], [11], [12], and references therein.

B. WOLA-OFDM Processing

Weighted overlap-and-add (WOLA) based OFDM (WOLA-OFDM) is a well-known low-complexity waveform processing technique to reduce the out-of-band (OOB) emissions in the Tx or to reduce signal cross-talk in the Rx [8], [9]. In WOLA-OFDM, the rectangular pulse shape of CP-OFDM is replaced with a longer and smoother pulse shape, which allows improved spectral containment performance. The gradually attenuating edges reduce the phase discontinuity between CP-OFDM symbols. Time-domain windowing with a window longer than the duration of the CP-OFDM symbol alone would cause extra overhead, and therefore overlap-and-add mechanism is also applied to remove this overhead. This introduces limited inter-symbol-interference between adjacent CP-OFDM symbols, which is controlled by the WOLA-OFDM window length.

In Tx-side WOLA-OFDM processing, the time-domain CP-OFDM symbols are extended by $L_{\mathrm{EXT},m}$ samples, multiplied element-wise by the time-domain window function, and concatenated using the overlap-and-add processing. Formally, the WOLA processing can be represented as $\mathbf{w} = \mathbf{K}_m\mathbf{x}_m$, where $\mathbf{K}_m$ is the following block-diagonal WOLA-processing matrix $\mathbf{K}_m = \mathrm{diag}\left(\mathbf{O}_{m,0}, \mathbf{O}_{m,1}, \ldots, \mathbf{O}_{m,R_m-1}\right)$ with $\mathbf{O}_{m,r} = \mathbf{D}_{\mathrm{TD},m}\mathbf{T}_{\mathrm{EXT},m}$. Here, $\mathbf{T}_{\mathrm{EXT},m}$ is the $(L_{\mathrm{WOLA},m}) \times (L_{\mathrm{OFDM},m} + L_{\mathrm{CP},m})$ time-domain cyclic extension matrix, whereas the time-domain windowing matrix $\mathbf{D}_{\mathrm{TD},m}$ of size $L_{\mathrm{WOLA},m} \times L_{\mathrm{WOLA},m}$ has the time-domain weights $w[\ell]$ on its diagonal and $L_{\mathrm{WOLA},m} = L_{\mathrm{OFDM},m} + L_{\mathrm{CP},m} + L_{\mathrm{EXT},m}$. In this study, a raised-cosine window is selected as the windowing function and corresponding weights can be expressed as [9]

$$w[\ell] = \begin{cases} 1 - \frac{1}{2}(1 + c[\ell]) & 0 \le \ell < \alpha L_{\mathrm{WOLA}}, \\ \frac{1}{2}(1 + c[\ell]) & (1-\alpha)L_{\mathrm{WOLA}} \le \ell < L_{\mathrm{WOLA}}, \\ 1 & \text{otherwise}, \end{cases} \quad (2)$$

where $c[\ell] = \cos(\pi\ell/(\alpha L_{\mathrm{WOLA}}))$ and α represents the roll-off factor.

IV. USRP-Based SDR Prototype Performance

In this section, the spectral containment performance results for FC-F-OFDM and WOLA-OFDM waveforms are provided. Performance is measured by both numerical evaluations and real-time experiments to provide a realistic and comprehensive comparison between these two waveforms. In the real-time measurements including a highly non-linear PA, UL transmission is considered and a wide range of different 5G NR numerologies and channel bandwidths are evaluated. With Matlab-based Tx chain and Tx signal quality numerical evaluations, results for ideal linear waveforms are obtained for reference purposes. Parameters used in numerical evaluations and prototype measurements are summarized in Table I. Channel bandwidths of 5 MHz, 20 MHz, and 100 MHz are considered, corresponding to low-, medium-, and high-class UEs. To push the limits of 5G NR, we have considered extreme spectrum utilization cases beyond 5G NR Release-15 numerology activating more PRBs than is currently allowed for 5G NR transmission bandwidth configurations [4]. Furthermore, in all cases, the measured Tx EVM was below 10.5%, following the 3GPP measurement guidelines defined in [4].

In order to quantify the spectral containment performance of the evaluated waveform candidates, two UE output RF spectrum emissions related metrics are evaluated as described in Section II-B. Firstly, 5G NR ACLR is evaluated by numerical evaluations and measured in real-time experiments by using the corresponding measurement tool of NI PXIe-5840 VST module [16]. Secondly, the OOB emissions are measured with channel bandwidth specific measurement bandwidths and compared to the corresponding OOB emission masks defined in [4]. In this paper, we show only results related to the OOB emissions within 1 MHz distance from the channel edge, because both waveform candidates were observed to perform similarly with larger distance from the channel edge and also in the spurious emission region. This is intuitive, because further away from the active allocation the performance is mainly dictated by the PA, and not by the waveform processing. In the case of OOB emissions, we define a Δ-metric representing the minimum difference between the OOB spectral emission mask and power spectral density (PSD) level of the waveform candidate in the measurement band. Quantifying the containment performance with respect to the spectral emission mask is important as it provides more information of the interference margin available for the implementation when considering emissions near the channel edge, and 5G NR ACLR metric does not provide this directly as it is a wideband measurement.

TABLE II: Numerical evaluation and real-time measurement results for NR ACLR.

Bandwidth	5 MHz				20 MHz						100 MHz			
SCS	15 kHz		30 kHz		15 kHz		30 kHz		60 kHz		30 kHz		60 kHz	
Number of allocated PRBs	25	**27**	11	**13**	106	**109**	51	**54**	24	**27**	273	**276**	135	**138**
$ACLR_{FC_{NUM}}$ (dBc)	85.7	**77.4**	82.3	**75.9**	95.0	**86.6**	91.0	**78.5**	87.0	**77.3**	98.7	**88.1**	95.2	**86.7**
$ACLR_{WOLA_{NUM}}$ (dBc)	71.6	**47.1**	67.7	**45.1**	88.2	**57.6**	83.8	**47.9**	77.3	**47.1**	98.6	**62.2**	92.2	**63.4**
$ACLR_{FC_{MEAS}}$ (dBc)	38.9	**38.2**	41.9	**38.3**	37.6	**35.0**	38.1	**35.9**	38.1	**37.1**	34.1	**34.0**	34.3	**34.1**
$ACLR_{WOLA_{MEAS}}$ (dBc)	38.9	**36.2**	40.5	**35.8**	37.4	**34.8**	38.1	**35.7**	38.0	**36.3**	33.9	**33.9**	34.3	**34.0**

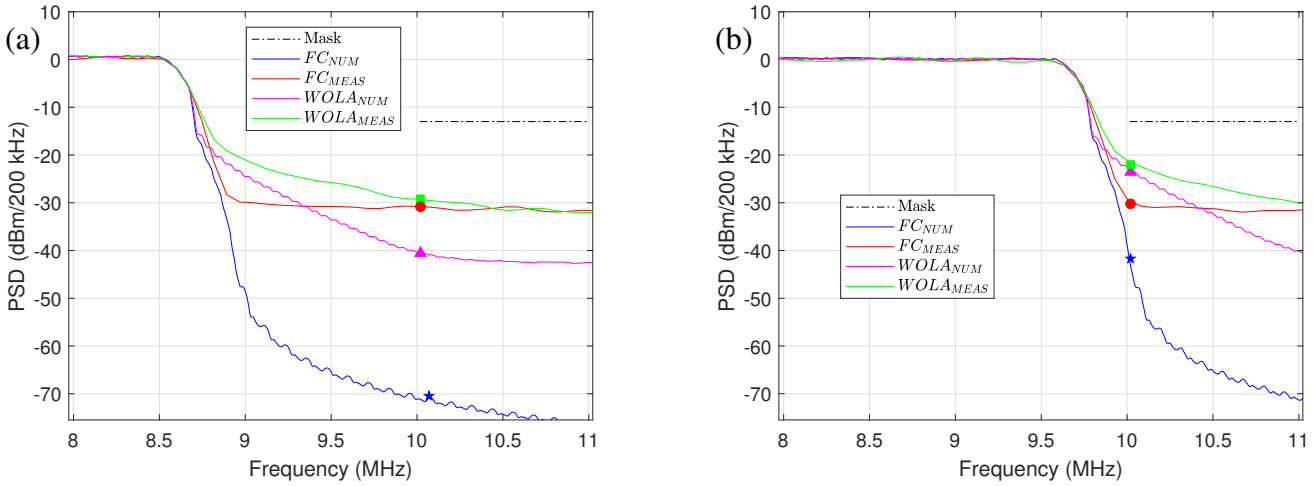

Fig. 4: Example of the numerical evaluation and real-time measurement based spectral containment results for FC-F-OFDM and WOLA-OFDM using a 20 MHz channel bandwidth with SCS of 60 kHz and allocation size of 24 PRBs and 27 PRBs shown in (a) and (b), respectively. Markers indicate the PSD values used for evaluating the corresponding Δ metrics for these particular cases, highlighting the minimum difference between the PSD response with respect to the emission mask. The numerical values of the corresponding Δ metrics are collected to Table III.

A. 5G NR ACLR Measurement Results

The 5G NR ACLR was evaluated numerically and measured in the real-time experiment and the results are collected for different channel bandwidths and SCSs in Table II. The results corresponding to extreme spectrum utilization are highlighted with bold font. In general, we note that in the numerical evaluation based cases, in the absence of nonlinear PA effects, the differences between FC-F-OFDM and WOLA-OFDM are significant. This also illustrates the level of difference, if the PA were operating in its more linear region. When extreme spectrum utilization is targeted, providing a view on the possible development of 5G NR or beyond 5G technologies, the ACLR differences between FC-F-OFDM and WOLA-OFDM become more pronounced. Typical to WOLA-OFDM, the spectral containment performance is degraded as the supported SCS is increased. This is due to the reduced length of the WOLA window that is relative to the CP-OFDM symbol length, and thus scales with the SCS. With FC-F-OFDM, the ACLR degradation is limited highlighting that FC-F-OFDM is more capable to push the spectrum utilization requirements of 5G NR even further while achieving similar performance in terms of NR ACLR with linear PA. These results also pronounce the potential of FC-F-OFDM processing for the base station transmitter, where the OOB emission requirements are significantly stricter than in the UE side, and this is considered as an important topic for future research. In the measured cases, FC-F-OFDM provides consistently better performance when compared to WOLA-OFDM, while both waveform candidates fulfill the required 5G NR ACLR of 30 dB for power class 3 devices PA [4].

B. 5G NR Out-of-Band Emission Performance

The UE OOB emission performance is evaluated both in numerical evaluations and real-time experiments, and example results are shown in Fig. 4. In this scenario, 20 MHz channel with 60 kHz SCS and measurement bandwidth of 200 kHz are considered by utilizing the current 5G NR Release-15 transmission bandwidth configuration of 24 PRBs in Fig. 4(a), and the extreme spectrum utilization case where 27 PRBs are allocated in Fig. 4(b). As it can be seen from Fig. 4(a), both FC-F-OFDM and WOLA-OFDM achieve the operating band unwanted emissions requirements, but the spectral containment of WOLA-OFDM is clearly worse. In the case of numerical evaluations, in the absence of nonlinear PA effects, FC-F-OFDM can provide approximately 31 dB better minimum interference margin compared to WOLA-OFDM. In the measurements, this difference is decreased mainly due to the distortion of the non-linear PA.

In Fig. 4(b), the performance with 27 allocated PRBs is shown, and the performance with WOLA-OFDM decreases significantly, because the time domain windowing is not able to suppress the leakage power near the active band. The minimum margin to the OOB emission mask with WOLA-OFDM is only 9 dB. In this case, FC-F-OFDM still provides a robust emission performance with 17 dB minimum margin to the 200 kHz OOB emission mask. It is also observed that WOLA-OFDM waveform provides a very similar performance both in numerical evaluations and real-time measurements due to the poor spectral containment near the active allocation. In the

TABLE III: Numerical evaluation and real-time measurement results for Δ metric defining the minimum margin between the OOB spectral emission mask and the measured PSD of the waveform candidate.

Bandwidth	5 MHz				20 MHz						100 MHz			
SCS	15 kHz		30 kHz		15 kHz		30 kHz		60 kHz		30 kHz		60 kHz	
Number of allocated PRBs	25	**27**	11	**13**	106	**109**	51	**54**	24	**27**	273	**276**	135	**138**
$\Delta_{\mathbf{FC_{NUM}}}$ **(dB)**	54.6	**34.9**	54.7	**34.3**	61.8	**50.5**	60.1	**46.7**	57.5	**28.8**	64.0	**54.8**	61.3	**42.5**
$\Delta_{\mathbf{WOLA_{NUM}}}$ **(dB)**	23.3	**11.2**	22.1	**10.9**	29.2	**18.6**	28.8	**15.7**	27.6	**10.6**	27.0	**17.8**	24.1	**13.3**
$\Delta_{\mathbf{FC_{MEAS}}}$ **(dB)**	19.7	**17.7**	18.5	**18.2**	18.7	**10.6**	18.5	**17.7**	17.8	**17.2**	18.7	**18.6**	18.8	**18.5**
$\Delta_{\mathbf{WOLA_{MEAS}}}$ **(dB)**	15.2	**7.9**	15.1	**8.4**	17.7	**9.6**	17.8	**10.8**	16.2	**9.0**	18.3	**15.3**	17.1	**12.6**

case of FC-F-OFDM, the signal has a clearly better spectral containment and also the interference floor induced by the Tx chain's non-linearities is clearly visible when comparing the simulated and measured results.

The defined Δ-metric describing the minimum margin between the transmitted signal PSD response and the OOB emission mask is evaluated both by numerical evaluation and real-time measurements for different channel bandwidths and SCS allocations, and the obtained results are summarized in Table III. The results corresponding to extreme spectrum utilization are highlighted with bold font. Starting with numerical evaluation results, the FC-F-OFDM's superiority over WOLA-OFDM waveform is clearly visible in all cases. In the cases of 5G NR Release-15 allocation or extreme spectrum utilization, the FC-F-OFDM provides at least 30 dB or 13 dB larger minimum margin in all evaluated configurations, respectively.

In the real-time measurement results, the Δ-metric shows that the difference between the waveform candidates decreases but FC-F-OFDM still provides clearly larger margin for implementation non-idealities than WOLA-OFDM. Also here the trend of increased performance difference between FC-F-OFDM and WOLA-OFDM with respect to the increased SCS is visible. In the case of extreme spectrum utilization, the minimum margin to the OOB emission mask is clearly degraded with WOLA-OFDM whereas FC-F-OFDM is able to maintain a considerably better margin despite the highly non-linear PA included in the measurement setup. For example, in the case of 5 MHz channel bandwidth and assuming 30 kHz SCS with extreme bandwidth utilization, FC-F-OFDM is able to provide 10 dB larger interference margin when compared to WOLA-OFDM.

V. Conclusion

In this work, a USRP-based SDR prototype implementing FC-F-OFDM processing for 5G NR wireless mobile communications was presented accompanied with a wide set of first-in-class UE transmitter RF emission results. The performance of FC-F-OFDM was compared with WOLA-OFDM in terms of 5G NR ACLR and out-of-band spectral emission requirements, following the latest 5G NR output RF spectrum emission definitions. The highly realistic uplink scenario was realized by applying an external wideband power amplifier to the USRP output to achieve the targeted 24 dBm amplifier output power. Despite the highly non-linear PA included in the measurements, FC-F-OFDM provided robust improvements in the spectral containment and clear benefits over the WOLA-OFDM processing in the ACLR and OOB spectral emission measurements. Furthermore, the evaluation set extended the current 5G NR transmission bandwidth configurations to further improve the spectral utilization beyond the current specifications. Especially, in these extreme spectral utilization cases the benefits of the FC-F-OFDM were pronounced compared to WOLA-OFDM. Also, FC-F-OFDM allowed to achieve similar performance results with 5G NR and beyond 5G parameterizations, highlighting the potential of the FC-F-OFDM solution to improve the spectral utilization and therefore the system throughput.

References

[1] S. Parkvall, E. Dahlman, A. Furuskar, and M. Frenne, "NR: The new 5G radio access technology," *IEEE Communications Standards Magazine*, vol. 1, no. 4, pp. 24–30, Dec. 2017.

[2] M. Shafi *et al.*, "5G: A tutorial overview of standards, trials, challenges, deployment, and practice," *IEEE J. Select. Areas Commun.*, vol. 35, no. 6, pp. 1201–1221, Jun. 2017.

[3] 3GPP TS 38.300, "NR; Overall description; Stage-2," Tech. Spec. Group Radio Access Network, Rel. 15 V15.4.0, Jan. 2019.

[4] 3GPP TS 38.101-1, "NR; User Equipment (UE) radio transmission and reception; Part 1: Range 1 Standalone," Tech. Spec. Group Radio Access Network, Rel. 15 V15.4.0, Jan. 2019.

[5] Y. Cai, Z. Qin, F. Cui, G. Y. Li, and J. A. McCann, "Modulation and multiple access for 5G networks," *IEEE Communications Surveys Tutorials*, vol. 20, no. 1, pp. 629–646, first quarter 2018.

[6] P. Guan, D. Wu, T. Tian, J. Zhou, X. Zhang, L. Gu, A. Benjebbour, M. Iwabuchi, and Y. Kishiyama, "5G field trials: OFDM-based waveforms and mixed numerologies," *IEEE J. Select. Areas Commun.*, vol. 35, no. 6, pp. 1234–1243, Jun. 2017.

[7] J. Yli-Kaakinen, T. Levanen, S. Valkonen, K. Pajukoski, J. Pirskanen, M. Renfors, and M. Valkama, "Efficient fast-convolution-based waveform processing for 5G physical layer," *IEEE J. Select. Areas Commun.*, vol. 35, no. 6, pp. 1309–1326, Jun. 2017.

[8] "Waveform Candidates, 3GPP TSG RAN WG1 meeting, #84b, R1-162199," Apr 2016.

[9] E. Bala, J. Li, and R. Yang, "Shaping spectral leakage: A novel low-complexity transceiver architecture for cognitive radio," *IEEE Vehicular Technology Magazine*, vol. 8, no. 3, pp. 38–46, Sep. 2013.

[10] X. Zhang, M. Jia, L. Chen, J. Ma, and J. Qiu, "Filtered-OFDM – Enabler for flexible waveform in the 5th generation cellular networks," in *Proc. IEEE Global Commun. Conf. (GLOBECOM)*, Dec. 2015, pp. 1–6.

[11] M. Renfors, J. Yli-Kaakinen, T. Levanen, M. Valkama, T. Ihalainen, and J. Vihriala, "Efficient fast-convolution implementation of filtered CP-OFDM waveform processing for 5G," in *Proc. IEEE Globecom Workshops (GC Wkshps)*, Dec. 2015, pp. 1–7.

[12] T. Levanen, J. Pirskanen, K. Pajukoski, M. Renfors, and M. Valkama, "Transparent Tx and Rx waveform processing for 5G new radio mobile communications," *IEEE Wireless Communications*, pp. 1–9, 2018.

[13] *Specifications USRP-2954*, National Instruments, 2018. [Online]. Available: http://www.ni.com/pdf/manuals/375725c.pdf

[14] *NRP-Z11 Power Meter*, Rohde & Schwarz, 2018. [Online]. Available: https://www.rohde-schwarz.com/fi/product/nrpz11-productstartpage_63493-8857.html

[15] *ZHL-4240+ Medium Power Amplifier*, Mini Circuits, 2018. [Online]. Available: http://www.minicircuits.com/pdfs/ZHL-4240+.pdf

[16] *Specifications VST PXIe-5840*, National Instruments, 2018. [Online]. Available: http://www.ni.com/pdf/manuals/376626c.pdf